Effect of Cu on Oxidation Behaviour of FCC Fe-Ni-Cr-Al and Ni-Cr-Al Based Alloys

Shigenari Hayashi[1], Daiki Kudo[1], Ryouta Nagashima[2] and Haruki Utsumi[1]

[1] Division of Material Science and Engineering, Graduate School of Engineering, Hokkaido University,

[2] School of Materials and Chemical Technology, Tokyo Institute of Technology.

[1] Kita13 Nishi8, Kita-ku, Sapporo, Hokkaido 060-8628, Japan

[2] 2-12-1 Ookayama, Meguro-ku, Tokyo, 152-8552, Japan

Abstract

The high-temperature oxidation behaviour of Fe-Ni-Cr-Al and Ni-Cr-Al alloys with and without Cu addition was investigated at 1000°C in air to determine the effect of Cu on the critical Al content necessary for forming an external Al_2O_3 scale. The oxidation mass gain of Fe-17Ni-17Cr-7.7Al-Cu and Ni-17Cr-10Al alloys was found to decrease with increased Cu content. An external Al_2O_3 scale developed when 5at%Cu and more and 10at%Cu and more was added to Fe-17Ni-17Cr-7.7Al and Ni-17Cr-10Al alloys, respectively. The beneficial effect of Cu is inferred to be due to decreased oxygen concentration at the alloy surface and enhanced Al outward diffusion.

Keywords: Al_2O_3-scale forming austenitic Fe-base alloy, Cu effect, critical Al content for Al_2O_3 scale formation

1. INTRODUCTION

Austenitic heat-resistant steels are expected to have excellent high-temperature mechanical properties at elevated temperatures. Most conventional austenitic heat-resistant steels form a Cr_2O_3 scale, which protects the steel in various high-temperature oxidation/corrosion environments. However, the thermal stability of Cr_2O_3 is inferior to Al_2O_3 in harsh environments when such environments contain aggressive species such as C, S, and Cl_2 at higher temperatures. Thus, using a protective Al_2O_3 scale is favoured as a protective oxide scale, because it provides better oxidation resistance in such aggressive environments. However, only ferritic steels and Ni-based alloys are available to form an Al_2O_3-scale in current heat-resistant alloy systems. For example, Fe-Cr-Al ferritic steels in particular, which form an Al_2O_3-scale, have excellent oxidation resistance and are widely used in various high-temperature components such as heating wire and metal foil for catalytic converters. However, in general the mechanical properties of

ferritic steels at high temperatures are not sufficient to make them for structural components. Thus, the only available alloys that form an Al_2O_3 scale that can be used at elevated temperatures higher than 700°C are Ni-based alloys. Although Ni-based alloys possess both excellent mechanical properties and oxidation performance, these alloys are much more expensive than other steels. Therefore, there is a need to develop Al_2O_3-scale forming austenitic heat resistant steels that can be produced by a conventional low-cost process such as a hot rolling.

Al_2O_3-scale forming austenitic steels require higher Al content for Al_2O_3 scale formation. This is because of the smaller diffusivity of solute elements in the fcc matrix. An addition of more than 20at%Al is necessary for Al_2O_3 scale to form on Fe-20%Ni alloy, and the required Al content increases with increasing Ni content [1, 2]. However, higher Al addition to austenitic steels results in the precipitation of bcc α-Fe and different compounds containing higher Al content such as a β-(Fe,Ni)Al and γ'-$(Ni,Fe)_3Al$ phases [3]. Due to the formation of β-Fe(Ni)Al-precipitates, Al content in the matrix γ-phase does not increase effectively. Consequently, the oxidation performance of alloys would not be improved as it is expected by the addition of Al with higher concentration. Brady et al. proposed Al_2O_3-scale forming austenitic steels that have good creep resistance due to the precipitation of different compounds: β-(Fe,Ni)Al, Laves-Fe_2(Mo,Nb), σ, and carbides [4, 5]. Brady et al. also found these steels have good oxidation resistance due to Nb addition, which significantly decreases the Al content by 2.5wt% to form an external Al_2O_3 scale on austenitic steels [6]. The β-NiAl-precipitates enhance the creep-resistance of ferritic [7] and austenitic [8] steels. However, as mentioned above, the formation of β-NiAl-precipitates might decrease the oxidation performance. In addition, manufacturing steels that contain β-Fe(Ni)Al precipitates by conventional methods such as a rolling would be difficult. Therefore, decreasing the critical Al content necessary for formation of an external Al_2O_3 scale on austenitic steels is necessary if new Al_2O_3-forming austenitic steels are to be developed.

In our preliminary investigation, we found Cu addition to austenitic steels is beneficial for Al_2O_3-scale formation. Moreover, Cu precipitation in austenitic stainless steels is known to improve high-temperature mechanical properties [9, 10]. Therefore, Cu addition to the austenitic substrate is expected to be beneficial for both the mechanical properties and oxidation performance at higher temperatures. In this study, we investigated the oxidation behaviour of Fe-Ni-Cr-Al alloys with and without Cu addition and tried to clarify the effect of Cu on the development of external Al_2O_3 scale. In order to assess the effect of Cu on oxidation behaviour, oxidation behaviour of simple Ni-Cr-Al alloys with and without Cu addition was also evaluated.

2. EXPERIMENTAL PROCEDURE

Fe-based fcc matrix Fe-Ni-Cr-Al-Zr and Ni-based Ni-Cr-Al-Zr alloys with and without different Cu contents were prepared by argon-arc melting using high purity metals (99.99%). Table 1 shows the nominal composition of the alloys used in this study. Zr was used to prevent spallation of the oxide scale [11, 12]. All the alloy ingots were homogenized at 1200°C for 24 h in a vacuum, ~5 x 10^{-3} Pa. Oxidation specimens approximately 1 mm thick were cut from the homogenized ingots and polished down to a 3-μm diamond paste. Prior to the oxidation experiments the specimens were ultrasonically cleaned in acetone.

The oxidation tests were carried out in a box furnace at 1000°C in air. Specimens were placed in individual alumina crucibles in order to collect spalled oxide scale and these crucibles were placed in the furnace hot zone. Specimens were heated to 1000°C at a rate of 10°C/min and oxidized for a given time up to 100 h after furnace temperature reached at 1000°C in air. After a given oxidation time, specimens were furnace cooled in air. The mass gain/loss was measured at room temperature with a precision balance, thereafter the specimens were returned to the furnace again at room temperature and oxidized again. With this "pseudo-cyclic" oxidation study, cyclic oxidation kinetics and spallation resistance of the oxide scale were evaluated. The initial oxidation behaviour of alloys, development of oxides during heating at a rate of 50°C/min followed by isothermal oxidation at 1000°C in air for 30 min, was performed by an in-situ high-temperature XRD in air by means of synchrotron radiation at the SPring-8 facility in Hyogo, Japan. The detailed experimental condition of in-situ HTXRD is described elsewhere [13]. Internal oxidation of several Ni-based alloys was also conducted at 1000°C. The samples were sealed in a vacuum quartz capsule with a mixture of Ni/NiO powders to avoid formation of Ni oxide and heated at 1000°C for different oxidation times of up to 64 h.

After the oxidation test, cross-sections of the oxide scale were observed by using a scanning electron microscope and the distribution of each element was analysed by using an electron probe micro analyser (EPMA). The oxide scale formed in the very initial oxidation stage was analysed by Glow Discharge Optical Emission Spectroscopy (GD-OES).

3. RESULTS

3.1 Oxidation kinetics of alloys

<Fe-based alloys>

Figure 1 shows the oxidation kinetics of Fe-based alloys used in this study. The oxidation of all the alloys was initially rapid and then followed by slower oxidation kinetics. The initial oxidation

mass gain of the alloys without Cu rapidly increased up to about 20 h and then transitioned to the slower oxidation stage. This initial oxidation mass gain decreased with increasing Cu content up to 5at%. The oxidation rate in the slower oxidation stage also decreased with increasing Cu content. Compared with the Fe-17Ni-17Cr-7.7Al-5Cu alloy, the initial oxidation mass gain of low Cr alloy (15at%) increased, but the rate of oxidation in the slower oxidation stage was slower. The oxidation kinetics of the low Al alloy, Fe-17Ni-17Cr-6Al-5Cu, increased and was similar to that of 7.7Al-3.5Cu alloy. Figure 2 shows the Effect of Cu content on the oxidation mass gain on a series of Fe-17Ni-17Cr-7.7Al-Cu alloys after 100 h. In this plot, the oxidation mass gains of 3.8 and 4.3Cu alloys for 100h were obtained by a continuous isothermal oxidation for 100h. Oxidation behaviour transitioned from less protective to protective behaviour at about 4at%Cu additions.

<Ni-based alloys>

Figure 3 shows the oxidation kinetics of Ni-based alloys. Similar to the oxidation behaviour of Fe-based alloys, initial rapid oxidation was observed for Ni-17Cr-10Al and Ni-17Cr-10Al-5Cu. The rate of oxidation of those alloys decreased after about 30h of oxidation. Higher Cu addition decreased this initial rapid oxidation, and transitioned to the slower oxidation stage in shorter oxidation time. The oxidation rate of alloys with 10 and 15Cu in the slower oxidation stage after 5h of oxidation was similar.

These results indicate that Cu addition is beneficial, as it decreases the initial oxidation mass gain for both Fe and Ni-based alloys, which indicate that Cu addition promotes the external Al_2O_3 scale formation. However, higher Cu addition was necessary for Ni-based alloys for this transition.

3.3 Cross-sections of oxide scale

<Fe-based alloys>

Figure 4 shows cross-sections of Fe-17Ni-17Cr-7.7Al-Cu alloys after oxidation for 100 h. A thick duplex oxide scale consisting of an outer Fe oxide scale containing NiO and an inner Cr_2O_3 layers was formed on the alloy without Cu. Al was oxidized internally to form Al_2O_3-precipitates below a Cr_2O_3 layer. Internal AlN-precipitate formation was also observed below the internal Al oxidation zone (Fig. 4a, d). An outer Fe-rich oxide scale was also observed on the alloy with 3.5at%Cu; however, it was thin and discontinuously distributed on the surface of the Cr_2O_3 scale. Internal Al_2O_3 and AlN-precipitates were also formed in this alloy, but internal Al_2O_3 became continuous below the needle-like internal Al_2O_3 zone (Fig. 4b, e, and 7a). An external Al_2O_3 scale

developed on the alloy with 5%Cu addition (Fig. 4c and f, Fig. 7b), and a very thin Fe-oxide layer was observed on the surface of the Al_2O_3 scale. Penetration of spike-shaped Al_2O_3 occurred locally along with bright contrast phase, which is considered to be ZrO_2 [14, 15], suggesting that Zr content in this alloy is slightly over-doping. EPMA analysis shown in Fig. 7 reveals that Cu content is constant and Cu oxide formation was not confirmed.

Figure 5 shows cross-sections of 6Al and 15Cr alloys after oxidation for 100 h. A thick duplex scale consisting of an outer Fe-Ni-oxide layer and an inner Cr_2O_3 layer formed on the alloy with 6 Al. Al was internally oxidized below the thick oxide scale. AlN formation below the internal Al_2O_3 precipitates was also observed. A continuous Al_2O_3 scale was formed on the 15Cr alloy, but the low Cr content resulted in the formation of an outer Fe(Ni) and Cr-rich oxide layers above the Al_2O_3 scale. The initial rapid increase in oxidation mass gain of this alloy could be due to formation of this outer Fe(Ni) and Cr-rich oxide layer; nevertheless, the inner Al_2O_3 layer was thin and formed over the entire surface of the alloy; therefore, the oxidation rate of this alloy decreased and became comparable to that of Fe-17Ni-17Cr-7.7Al-5Cu alloy. Figure 6 shows the cross-sections of Fe-24Ni-17Cr-7.7Al alloy after 100h of oxidation. The oxide scale formed on this alloy was almost same as the oxide scale formed on Fe-17Ni-17Cr-7.7Al. Higher Ni content did not improve the oxidation behaviour, indicating that Cu addition is beneficial for establishment of an Al_2O_3 scale.

<Ni-based alloys>

Figure 8 shows cross-sections of Ni-17Cr-10Al alloy and Ni-17Cr-10Al with 5, 10, and 15Cr alloys after 100h of oxidation. Ni-17Cr-10Al and 5Cu alloys formed a thick oxide scale. Based on the EPMA analysis shown in Fig. 9, the thick oxide scale consists of an NiO, Cr_2O_3, $NiCrAl_2O_4$, and Al_2O_3 layers in this order. However, 10 and 15Cu alloys formed a very thin oxide scale. This oxide scale consisted of an outer thin $NiAl_2O_4$ and an inner Al_2O_3 layers. Similar to Fe-based alloys, penetration of Al_2O_3 into the alloy substrate was observed along with the Zr internal oxide precipitates.

Figure 10 shows the cross-sections of Ni-based alloys after 4h of oxidation. A duplex oxide scale with an outer NiO and an inner Cr_2O_3 layers was formed on the Ni-17Cr-10Al and -5Cu alloys, although most of the outer NiO scale formed on Ni-17Cr-10Al was spalled. An internal Al_2O_3 zone was observed in both alloys, but internal Al_2O_3 precipitates were connected to form a continuous Al_2O_3 layer on Ni-17Cr-10Al-5Cu. The oxide structure formed on 10Cu alloy was similar to that formed on 5Cu alloy but the oxide scale was much thinner than that formed on 5Cu.

A continuous Al_2O_3 scale was developed on 10Cu alloy at this oxidation time. An external Al_2O_3 scale, which contains $NiAl_2O_4$ precipitates (bright contrast) in the outer part of oxide scale was developed on the alloy with 15Cu.

Because internal Al_2O_3 precipitates became a continuous Al_2O_3 layer with increasing Cu contents, it is apparently that Cu addition promotes the transition from internal to external Al_2O_3 scale formation, i.e., decreases the critical Al content to form an external Al_2O_3 scale.

3.4 Initial Oxidation Behaviour of Ni-based alloys

Figure 11 shows the initial oxidation behaviour of Ni-Cr-Al and Ni-Cr-Al-15Cu alloys obtained by in situ high-temperature XRD by means of synchrotron source. During heating to 1000° C, both alloys initially formed NiO, however, signals from CuO were also observed on the 15Cu alloy just before NiO formation. The greater NiO peak shift to the lower two theta angle around $2\theta = 23.7°$ during heating on the 15Cu alloy comparing to the Ni-Cr-Al suggests dissolution of Cu-oxide in the NiO. Then the position of NiO peak moved back to the higher two theta angle due to the formation of $NiAl_2O_4$. Once $NiAl_2O_4$ was formed, signals from Cu-oxides disappeared. The signals from $NiAl_2O_4$ were not observed on Ni-Cr-Al alloy, but $NiCr_2O_4$ was detected after Cr_2O_3 formation on this alloy without Cu. The signal from Al_2O_3 was also detected on this alloy, but where observed later than that on the alloy with Cu. Those differences, as well as the cross-section after 4h in Fig. 10a, indicate that the signal of Al_2O_3 observed on the Ni-Cr-Al alloy originates from internal Al_2O_3 precipitates. Thus, it is apparent that Ni-Cr-Al-15Cu alloy formed an Al_2O_3 scale below the NiO scale during the heating stage. However, Cu addition did not change the very initial transient oxidation behavior. Although Cu-oxide formation was observed on Ni-Cr-Al-Cu alloy, both alloys initially formed NiO. Therefore, the beneficial effect of Cu could be attributed to factors such as changes in oxygen solubility and diffusivities of oxygen and Al in the alloy substrate as discussed below.

4. DISCUSSION

Cu addition was found to be beneficial for external Al_2O_3 scale formation on both the Fe and Ni-based FCC alloy groups. Comparing the oxidation behaviour of Fe-17Ni-17Cr-7.7Al-5Cu (Ni+Cu=22at%) with Fe-24Ni-17Cr-7.7Al also supports the finding that Cu addition is beneficial to the formation of Al_2O_3 scale because replacement of Ni with Cu in the alloys significantly improved the oxidation performance. In case of Ni-based alloys, higher Cu additions were necessary to form an external Al_2O_3 scale even though alloys contained higher Al contents, 10%

higher than that of Fe-based alloys; however, the beneficial effect of Cu was also confirmed. In the following section, we initially discuss the effect of Cu on Al_2O_3 scale formation on Ni-based alloys.

The beneficial effect of Cu on the formation of an external Al_2O_3 scale in Ni-based alloys was confirmed by Niu et al. [16, 17]. They reported an external Al_2O_3 scale formation on the Ni-45Cu-10Al at 900° C in O_2, but the oxide scale formed on Ni-30Cu-10Al alloy was a duplex consisting of an outer Ni-Al spinel and inner Al_2O_3 layers. Formation of an internal Al_2O_3 zone was also formed locally below the Al_2O_3 scale on 30Cu alloy. It is known that 10at%Al is not sufficient to form an external Al_2O_3 scale on Ni-Al alloy [18, 19]. They inferred that this beneficial effect of Cu is attributed to increasing Al diffusion in the substrate with higher Cu contents, which decreases the critical Al content to form an external Al_2O_3 scale. They also evaluated the critical Al content to form an external Al_2O_3 scale, which is smaller for Cu-Al alloys thanfor Ni-Al alloys, however, assessment of the critical Al content on ternary Ni-Cu-Al system was not conducted.

The transition from internal to external Al_2O_3 scale formation is attributed to the higher permeability of Al, $N_{Al}D_{Al}$, than that of oxygen, N_OD_O, in the alloy substrate [20]. Cu may have an effect on those permeabilities; however, to our knowledge no studies have reported on the permeability of O and Al in both the Fe-Ni-Cr-Al-Cu and Ni-Cr-Al-Cu alloys.

The effect of Cu on the concentration of oxygen, No, in Ni-Cu alloy can be evaluated by eq(1) which was proposed by Jacobs and Alcock [21].

$$N_{Ni}\left(\frac{\gamma_{Ni(Ni-Cu)}^{\alpha}}{\gamma_{O(Ni)}^{1/n}}\right)+N_{Cu}\left(\frac{\gamma_{Cu(Ni-Cu)}^{\alpha}}{\gamma_{O(Cu)}^{1/n}}\right)=\left(\frac{1}{\gamma_{O(Ni-Cu)}^{1/n}}\right) \quad (1)$$

where $\gamma_{Ni(Ni-Cu)}$ and $\gamma_{Cu(Ni-Cu)}$ are the activity coefficients of Ni and Cu in the Ni-Cu alloy, respectively. $\gamma_{O(i)}$ (i = Ni, Cu, or Ni-Cu) is the oxygen activity coefficient. N_{Ni} and N_{Cu} are the mole fraction of Ni and Cu, respectively. α is the degree to which metal-metal bods are weakened and n is the number of bonds made by oxygen [x]. Then the oxygen mole fraction, N_O can be calculated at given oxygen potential P_{O2} by following equation with the Seivert's law.

$$K_s=\frac{N_O}{P_{O_2}^{1/2}}=\frac{1}{\gamma_O} \quad (2)$$

Figure 12 shows the oxygen mole fraction as a function of Cu contents in Ni-Cu alloy. The oxygen mole fraction was calculated using eq(1) with α=1/2 and n=4 [21] at the oxygen partial pressure of Ni/NiO equilibrium at 1000° C, P_{O2} = 4.68 x 10^{-12} atm, with $\gamma_{O(Ni)}$=0.0047 and $\gamma_{O(Cu)}$=6.9982, which were calculated from [22-24]. The activity coefficients, $\gamma_{Ni(Ni-Cu)}$ and $\gamma_{Cu(Ni-Cu)}$ were obtained from [25]. The oxygen mole fraction is shown to decrease with

increasing Cu contents. The oxygen mole fraction in 15Cu alloy is about 60% of that in Ni.

No data of diffusivity of oxygen and aluminum are also available for the Ni-Cu-Al system. Therefore, we conducted internal oxidation experiments of ternary Ni-Cu-Al alloys in Rhines pack method at the oxygen partial pressure of the Ni/NiO equilibrium at 1000° C. Figure 13 shows the internal oxidation kinetics of Ni-3Al and Ni-3Al-30Cu alloys. Internal oxidation kinetics of 30Cu alloy were higher than that of Ni-3Al. The cross-sections of alloys after 64h of oxidation are shown in Fig. 14, revealing that rod-like internal Al_2O_3 precipitates were formed on both alloys, with a higher volume fraction of internal precipitates formed in 30Cu than that formed in Ni-3Al alloy (Fig. 15). Al depletion was observed in both alloys below the internal oxidation zone as shown in Figs. 14c and d, and the thickness of the Al depletion zone was greater for 30Cu alloy. This agrees with higher volume fraction of internal precipitates in 30Cu alloy, suggesting that the outward Al diffusion in 30Cu alloy was higher than that in Ni-3Al alloy.

Under the condition that the outward Al diffusion cannot be neglected, the internal oxidation kinetics are given by [20] with the effective diffusion coefficient of oxygen, $D_{O,eff}$.

$$X = \frac{\sqrt{\pi} t^{1/2} N_O^{(s)} D_{O,eff}}{2\nu N_{Al}^{(0)} D_{Al}^{1/2}} \quad (3)$$

where $N_O^{(s)}$ and $N_{Al}^{(0)}$ are the oxygen mole fraction at the surface and the initial Al mole fraction in the alloy, $D_{O,eff}$ and D_{Al} are the effective oxygen and aluminium diffusion coefficients, respectively. ν is the ratio of oxygen to metal atoms in the oxide and is 1.5 for Al_2O_3. Because the rod-like internal precipitates which formed perpendicularly to the surface, the oxygen diffusion along the Al_2O_3/substrate interface is enhanced. The effective diffusion coefficient of oxygen, $D_{O,eff}$, can be calculated by [26] with the assumption of a cylindrical rod-like Al_2O_3 precipitate with a radius of *r*.

$$\frac{D_{O,eff}}{D_O} = 1 + \left[\frac{D_{O,i}\delta_i}{D_o}\frac{3}{r} - 1\right]\frac{V_{ox}}{V_{alloy}} N_{Al2O3} \quad (4)$$

where N_{Al2O3} is mole fraction of Al_2O_3 in the substrate and δ_i is the width of the internal Al_2O_3/substrate interface. D_O and $D_{O,i}$ are the diffusion coefficients of oxygen in the alloy substrate and at the internal Al_2O_3/substrate interface, and V_{Ox} and V_{alloy} are molar volume of Al_2O_3 and alloy, respectively. With the assumption that all parameters except $D_{O,eff}$ and D_O in eq(4) are constant, the effective diffusion coefficient of oxygen in 30Cu alloy must be higher than that in Ni-3Al alloy because of its higher N_{Al2O3}. In most of internal oxidation studies of Fe-Al and Ni-Al alloys, the internal oxidation kinetics decrease with increases in Al content [27, 28], because Al_2O_3 precipitates become a barrier for the oxygen inward diffusion due to higher volume

fraction of internal precipitates. However, in the present study, the internal oxidation kinetics of 30Cu alloy with higher N_{Al2O3} were higher than that of Ni-3Al. This opposite trend on internal oxidation kinetics was also observed in the study of oxidation of Ni-low Al alloys in N_2-20%O_2 at 800° C [29], and can be explained when D_O is much smaller than $D_{O,i}$ in Cu containing alloys, i.e., contribution of the oxygen diffusion flux along the interface become much stronger in the alloy with Cu.

Using eqs (3) and (4), the effect of Cu on the oxygen and Al diffusion coefficients can be evaluated, however, because each coefficient depends on Cu content, evaluation of the individual diffusion coefficients is not possible. A more detailed internal oxidation study as well as a diffusion study in the Ni-Cu-Al system are necessary for further discussion. However, it is apparent that Cu addition reduces the oxygen mole fraction in the alloy surface (Fig. 12) and enhance the Al outward diffusion. Those factors can promote an external Al_2O_3 scale formation on Cu containing alloys.

Doi et al. reported Cu segregation at the Cr_2O_3/substrate interface on Ni-Cr alloy after very short-term oxidation, 300s, at 650° C in 60%CO-26%H_2-11.5%CO_2-2.5%H_2O by the hard X-ray photoelectron spectroscopy by means of synchrotron source [30]. The thickness of Cu-segregation layer formed below the Cr_2O_3 scale was about 0.25nm and Cu content was about 50%. Although the alloy and oxidation condition in the present study is different, Cu segregation at the scale/alloy interface in the initial oxidation stage in the present study is expected, because Cu cannot be oxidized once a NiO scale is formed as shown in Fig. 11. Once Cu is segregated, it further decreases the surface oxygen mole fraction and could increase Al diffusion. Those factors promote an Al_2O_3 scale formation.

Cu addition in Fe-based alloys was more effective than Ni-based alloys. The solubility of oxygen in FCC Fe-Ni system is reported to increase with increase in Fe content [31]. The diffusion coefficient of oxygen at 1000°C in FCC Fe, 2.0×10^{-7} cm^2/s [27] is much higher than that in Ni, 9.1×10^{-9} cm^2/s [22]. Although the available diffusion coefficients in Fe-Ni-Al system are only at 1000°C, Fe/Ni ratio does not affect the main-term interdiffusion coefficient, $\widetilde{D}_{AlAl}^{Fe}$ [32, 33]. This suggest opposite oxidation behavior that the Fe-Ni-Al system requires higher critical Al content to form an external Al_2O_3 scale. However, it was reported that the cross-term interdiffusion coefficient of Al, $\widetilde{D}_{AlNi}^{Fe}$ is negative and has a same order to the main-term diffusion coefficient in [32, 33]. Figure 16 shows the GD-OES depth profile of Fe-17Ni-17Cr-7.7Al-7Cu alloy after 30s of oxidation in air at 1000°C. Ni-enrichment was observed just below the oxide scale, this would be caused by Fe-depletion due to formation of an Fe-oxide in the transient oxidation period.

As it proposed from the oxidation of Ni-Pt-Al alloys [34, 35], the outward Al diffusion at the subsurface region would be enhanced due to the negative cross-term coefficient and Ni-enrichment, which could further decrease the critical Al content to form the external Al_2O_3 scale on Fe-based alloys.

5. CONCLUSIONS

The oxidation of austenitic Fe-Ni-Cr-Al with and without Cu addition was carried out at 1000°C in air, and effect of Cu on the development of Al_2O_3 scale was investigated. The results obtained are summarized as follows.

1) Oxidation kinetics of Fe-Ni-Cr-Al and Ni-Cr-Al alloys decreased with the increase in alloy Cu content. An external Al_2O_3 scale developed with the addition of 4at%Cu and 10at%Cu on the Fe-17Ni-17Cr-7.7Al and Ni-17Cr-10Al alloys, respectively.
2) The beneficial effect of Cu is attributed to decrease in the oxygen mole fraction in the alloy surface and enhanced Al outward diffusion.
3) The cross-term effect of Ni on Al outward diffusion in Fe-Ni-Cr-Al-Cu alloy could further decrease the Al and Cu contents to formation of the external Al_2O_3 scale.

Acknowledgements

This study was supported in a part by JSPS KAKENHI Grant Number JP15H04153. The synchrotron radiation experiments were performed at BL46 of SPring-8 with the approval of the Japan Synchrotron Radiation Research Institute (JASRI) (Proposal No. 2015B1635 and 2016A1806).

REFERENCE

[1] P. Tomaszewicz and G.R. Wallwork, Corrosion-NACE, 40 (1984) 152-157.

[2] M. Sakiyama, P. Tomaszewicz, and G.R. Wallwork, Oxid. Met., 13 (1979), 311-330.

[3] L. Eleno, K. Frisk, and A. Schneider, Intermetallics, 14 (2006) 1276-1290.

[4] M.P. Brady, Y. Yamamoto, M.L. Santella, P.J. Maziasz, B.A. Pint, C.T. Liu, Z.P. Lu, and H. Bei, JOM, 60 (2008) 12-18.

[5] Y. Yamamoto, M.L. Santella, M.P. Brady, H. Bei and P.J. Maziasz, Metal. Mater. Trans. A, 40A (2009) 1868-1880.

[6] M.P. Brady, Y. Yamamoto, M.L. Santella, and B.A. Pint, Scripta Mater., 57 (2007) 1117-1120.

[7] Z. Sun, C.H. Liebscher, S. Huang, Z. Teng, G. Song, G. Wang, M. Asta, M. Rawlings, M.E.

Fine, and P.K. Liaw, Scripta Mater. 68 (2013) 384-388.
[8] D.V.V. Satyanarayana, G. Malakondaiah, and D.S. Sarma, Mater. Sci. Eng., A323 (2002) 119-128.
[9] C. Chi, H. Yu, J. Dong, W. Liu, S. Cheng, Z. Liu, and X. Xie, Prog. Natural Sci., 22 (2012) 175-185.
[10] K. laha, J. Kyono, and N. Shinya, Scripta Mater., 56 (2007) 915-918.
[11] K. Wambach, J. Peters, and H.J. Grabke, Mater. Sci. Eng., 88 (1987) 205-212.
[12] E.C. Dickey, B.A. Pint, K.B. Alexander, and I.G. Wright, J. Mater. Res., 14 (1999) 4531-4540.
[13] S. Yoneda, S. Hayashi, I. Saeki and S. Ukai, Oxid. Met., 86 (2016) 357-370.
[14] C.H. Xu, W. Gao, and H. Gong, Intermetallics 8 (2000) 769-779.
[15] J. Klöwer, Mater. Corr., 51 (2000) 373-385.
[16] Y. Niu, J.H. Xiang, and G. Gesmundo, Oxid. Met., 60 (2003) 293-313.
[17] J.H. Xiang, G. Gesmundo, and Y. Niu, Corr. Sci., 46 (2004) 2025-2039.
[18] X.J. Zhang, S.Y. Wang, F. Gesmundo, and Y. Niu, Oxid. Met., 65 (2006) 151-165.
[19] F.S. Pettit, Trans. Met. Soc. AIME, 239 (1967) 1296-1305.
[20] C. Wagner, Z. Ekektrochem., 63 (1959) 772-782.
[21] K.T. Jacob and C.B. Alcock, Acta Metall., 20 (1972) 221-232.
[22] J-W. Park and C.J. Altstetter, Metal. Metall. Trans. A, 18A (1987) 43-50.
[23] B. Hallstedt, D. Risold, and L.J. Gauckler, J. Phase Equilibria, 15 (1994) 483-499.
[24] M.L. Narula, V.B. Tare, and W.L. Worrell, Metall. Trans. B, 14B (1983) 673-677.
[25] T. Oishi, S. Tagawa, and S. Tanegashima, Mater. Trans., 44 (2003) 1120-1123.
[26] D.P. Whittle, Y. Shida, G.C. Wood, F.H. Stott, and B.D. Bastow, Phi. Mag. A, 46 (1982) 931-949.
[27] J. Takada, S. Yamamoto, S. Kikuchi, and M Adachi, Metall. Trans. A, 17A (1986) 221-229.
[28] A. Martinez-Villafane, F.H. Stott, JH.G. Chacon-Nava, and G.C. Wood, Oxid. Met., 75 (2002) 267-279.
[29] S. Hayashi, S. Narita, and T. Narita, Oxid. Met., 66 (2006) 191-207.
[30] T. Doi, K. Kitamura, Y. Nishiyama, N. Otsuka, T. Kudo, M. Sato, E. Ikenega, S. Ueda, and K. Kobayashi, Surf. Interface Anal., 40 (2008) 1374-1381.
[31] D. Jullian, J. Zhan, D. B. Hibbert, and D.J. Young, J. Alloy Comp., 732 (2018) 646-654.
[32] G.H. Cheng and M.A. Dayananda, Metall. Trans. A, 10A (1979) 1415-1419.
[33] Y.H. Sohn and M.A. Dayananda, Metall. Mater. Trans. A, 33A (2002) 3375-3392.

[34] S. Hayashi, T. Narita, and B. Gleeson, Materials Science Forum, 522-523 (2006) 229-238.
[35] S. Hayashi, W. Wang, D.J. Sordelet, and B. Gleeson, Metal. Mater. Trans. A, 36A (2005) 1769-1775.

Caption list

Fig.1 Oxidation kinetics of Fe-based alloys at 1000° C in air
Fig. 2 Oxidation mass gain of Fe-17Ni-17Cr-7.7Al-Cu alloys as a function of Cu contents
Fig. 3 Oxidation kinetics of Ni-based alloys at 1000° C in air
Fig. 4 Cross-sections of oxide scale formed on (a)(d) Fe-17Ni-17Cr-7.7Al, with (b)(e) 3.5Cu and (c)(f) 5Cu alloys after 100h of oxidation in air at 1000° C, (d)(e)(f) are enlarged images of boxed areas in (a)(b)(c)
Fig. 5 Cross-sections of oxide scale formed on (a) Fe-17Ni-17Cr-6Al-5Cu and (b) Fe-17Ni-15Cr-7.7Al-5Cu after 100h of oxidation in air at 1000° C, (c) is enlarged image of (b)
Fig. 6 Cross-sections of oxide scale formed on Fe-24Ni-17Cr-7.7Al. (b) is enlarged image of (a).
Fig. 7 EPMA concentration profiles of each element of (a) Fe-17Ni-17Cr-7.7Al-3.5Cu and (b) Fe-17Ni-17Cr-7.7Al-5Cu after 100h of oxidation in air at 1000° C
Fig. 8 Cross-sections of oxide scale formed on (a) Ni-17Cr-10Al, with (b) 5Cu, (c) 10Cu, and (d) 15Cu alloys after 100h of oxidation in air at 1000° C
Fig. 9 EPMA concentration profiles of each element of 17Ni-17Cr-10Al after 100h of oxidation in air at 1000° C
Fig. 10 Cross-sections of oxide scale formed on (a) Ni-17Cr-10Al, with (b) 5Cu, (c) 10Cu, and (d) 15Cu alloys after 4h of oxidation in air at 1000° C
Fig. 11 In-situ HT-XRD patterns of (a)Ni-17Cr-10Al and (b)Ni-17Cr-10Al-15Cu alloys during heating followed by isothermal oxidation in air at 1000° C
Fig. 12 Effect of Cu on the oxygen solubility in Ni-Cu system at 1000° C
Fig. 13 Internal oxidation kinetics of Ni-3Al and Ni-3Al-30Cu at 1000° C in Ni/NiO mixture
Fig. 14 Cross-sections of (a)Ni-3Al and (b)Ni-3Al-30Cu after internal oxidation for 64h at 1000° C
Fig. 15 Volume fraction of internal Al_2O_3 precipitates formed in Ni-3Al and Ni-3Al-30Cu alloys
Fig. 16 GD-OES concentration profiles of each element of (a) Fe-17Ni-17Cr-7.7Al and (b) Fe-

17Ni-15Cr-7.7Al-7Cu after 30s of oxidation in air at 1000° C

Table 1 Composition of alloys (nominal in at%)

Table 1 Composition of alloys (nominal in at%)

	Fe	Cr	Ni	Al	Cu	Zr
Fe-based	Bal.	17	17	7.7	-	0.03
					3.5	
					3.8	
					4.3	
					5	
					7	
				6	5	
			24	7.7	-	
		15	17	7.7	5	
Ni- based	-	17	Bal.	10	-	
					5	
					10	
					15	

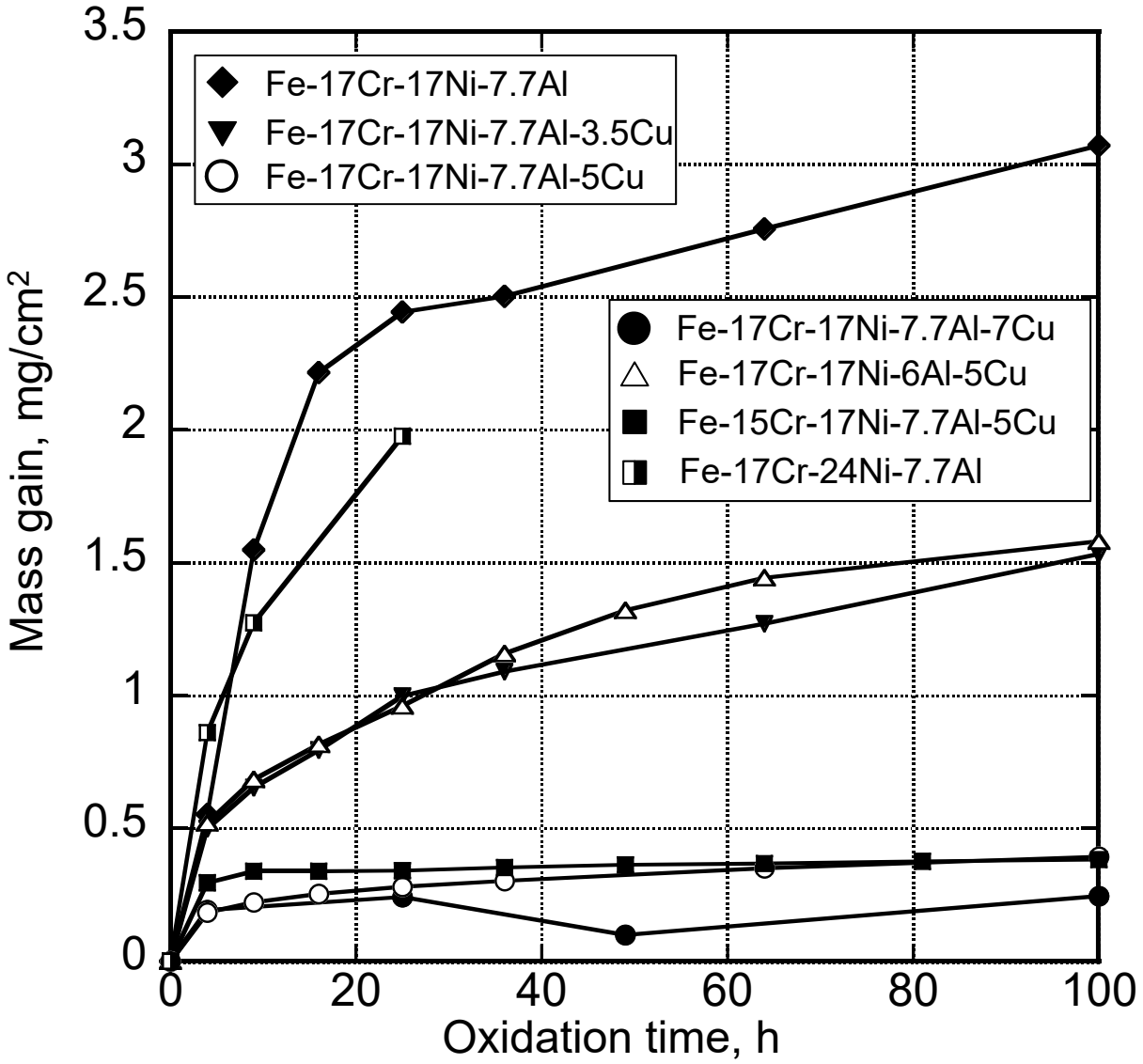

Fig. 1 Oxidation kinetics of Fe-based alloys at 1000°C in air

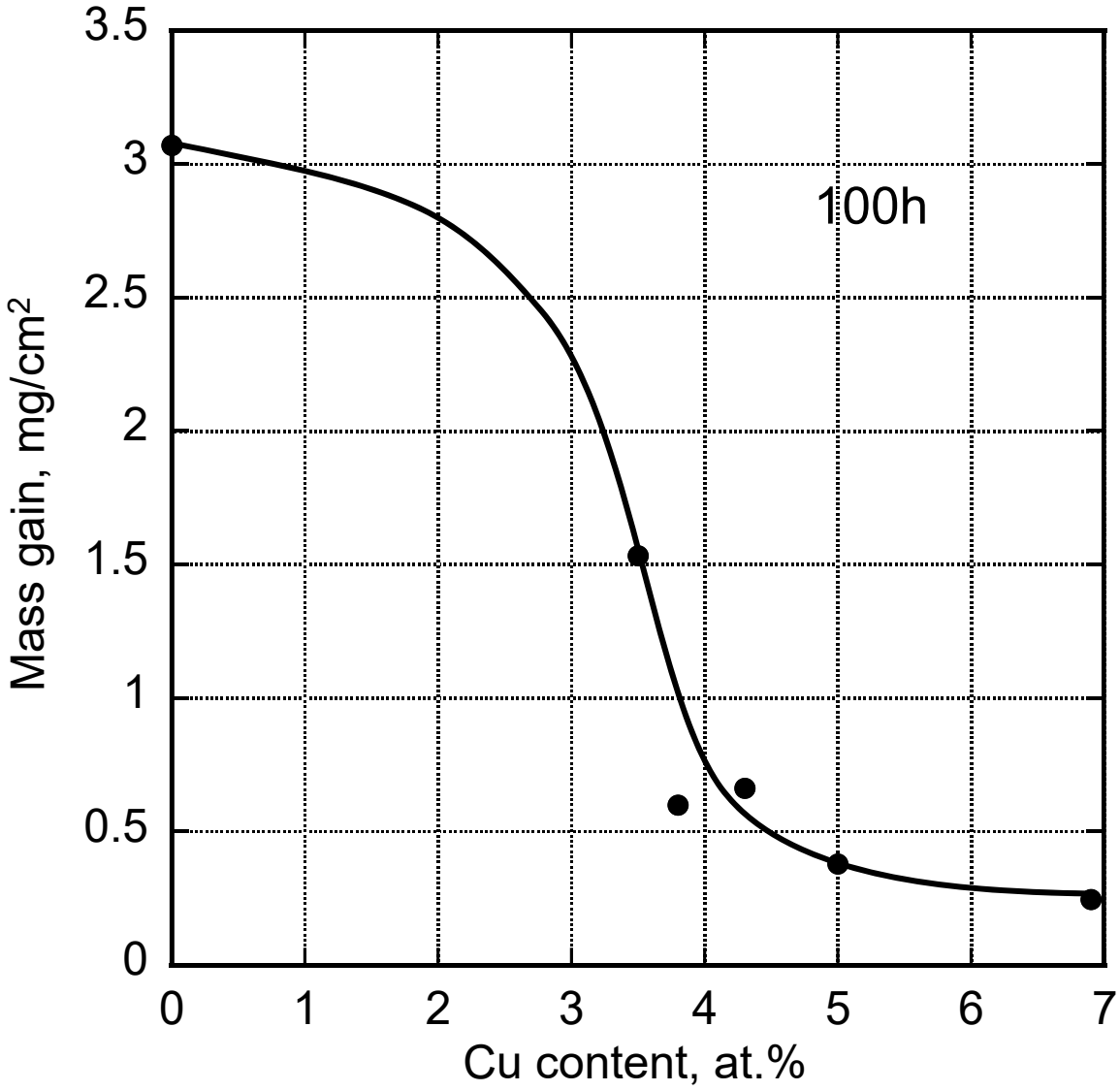

Fig. 2 Oxidation mass gain of Fe-17Ni-17Cr-7.7Al-Cu alloys as a function of Cu contents

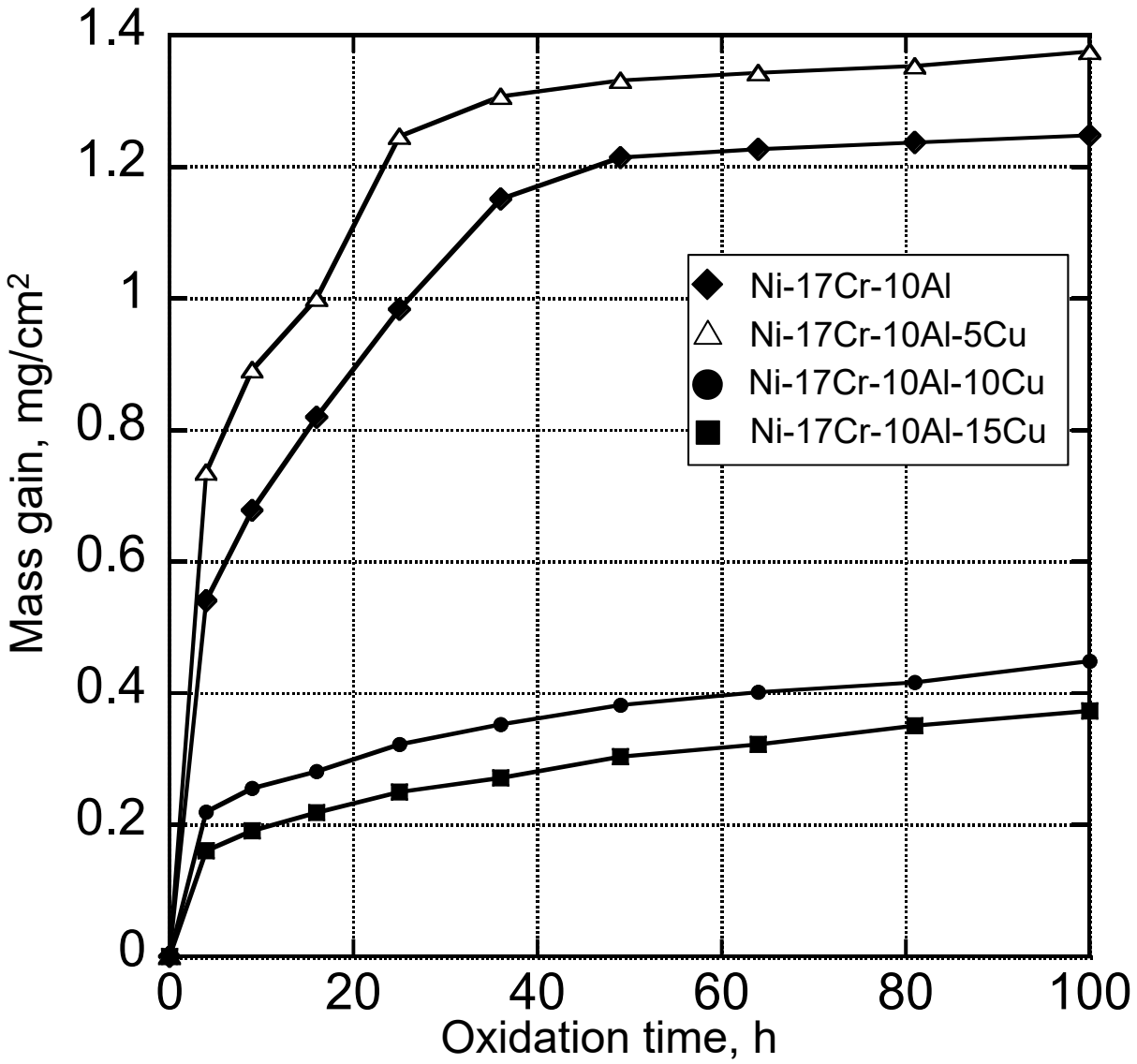

Fig. 3 Oxidation kinetics of Ni-based alloys at 1000°C in air

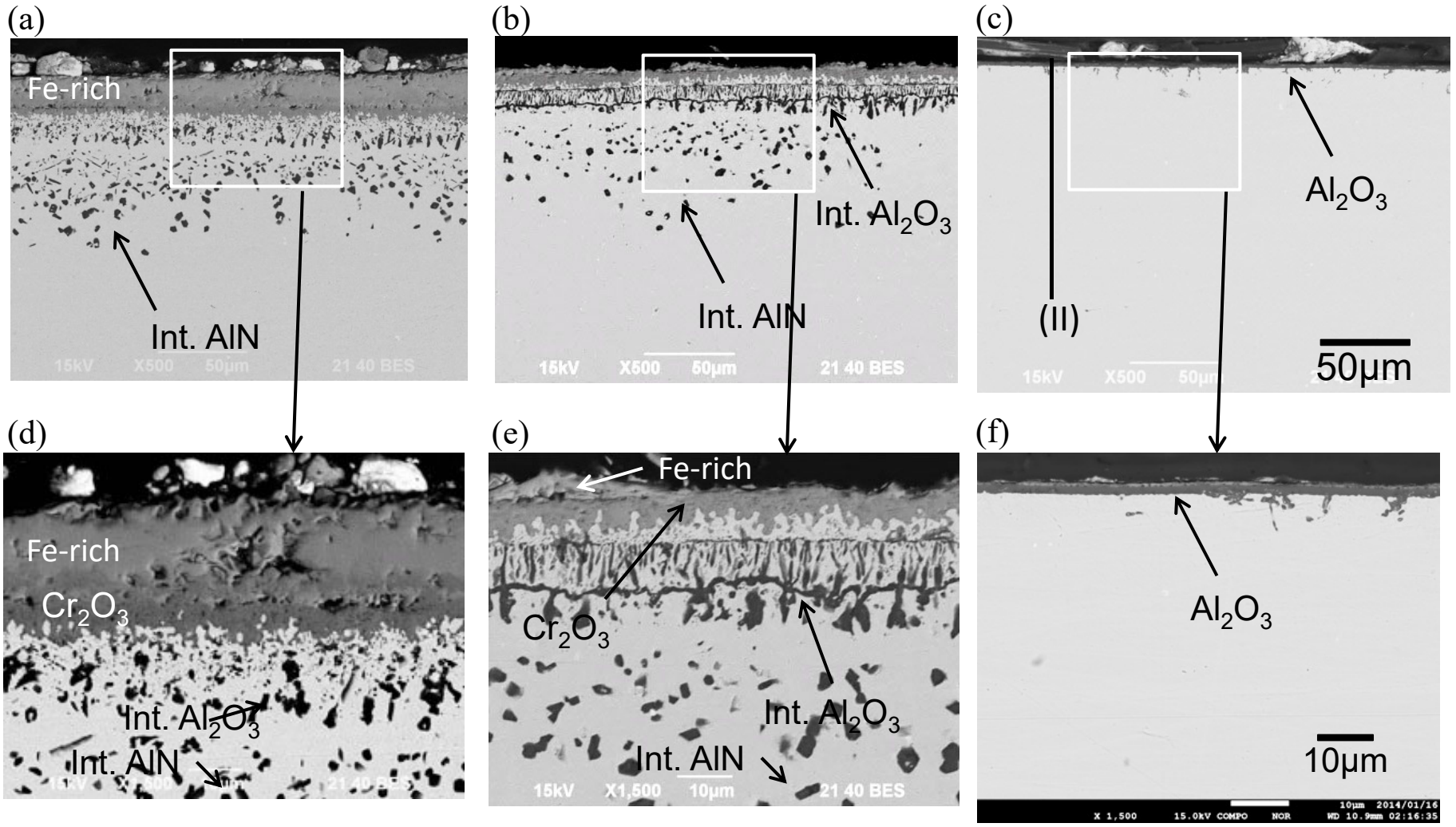

Fig. 4 Cross-sections of oxide scale formed on (a)(d) Fe-17Ni-17Cr-7.7Al, with (b)(e) 3.5Cu and (c)(f) 5Cu alloys after 100h of oxidation in air at 1000 °C, (d)(e)(f) are enlarged images of boxed areas in (a)(b)(c)

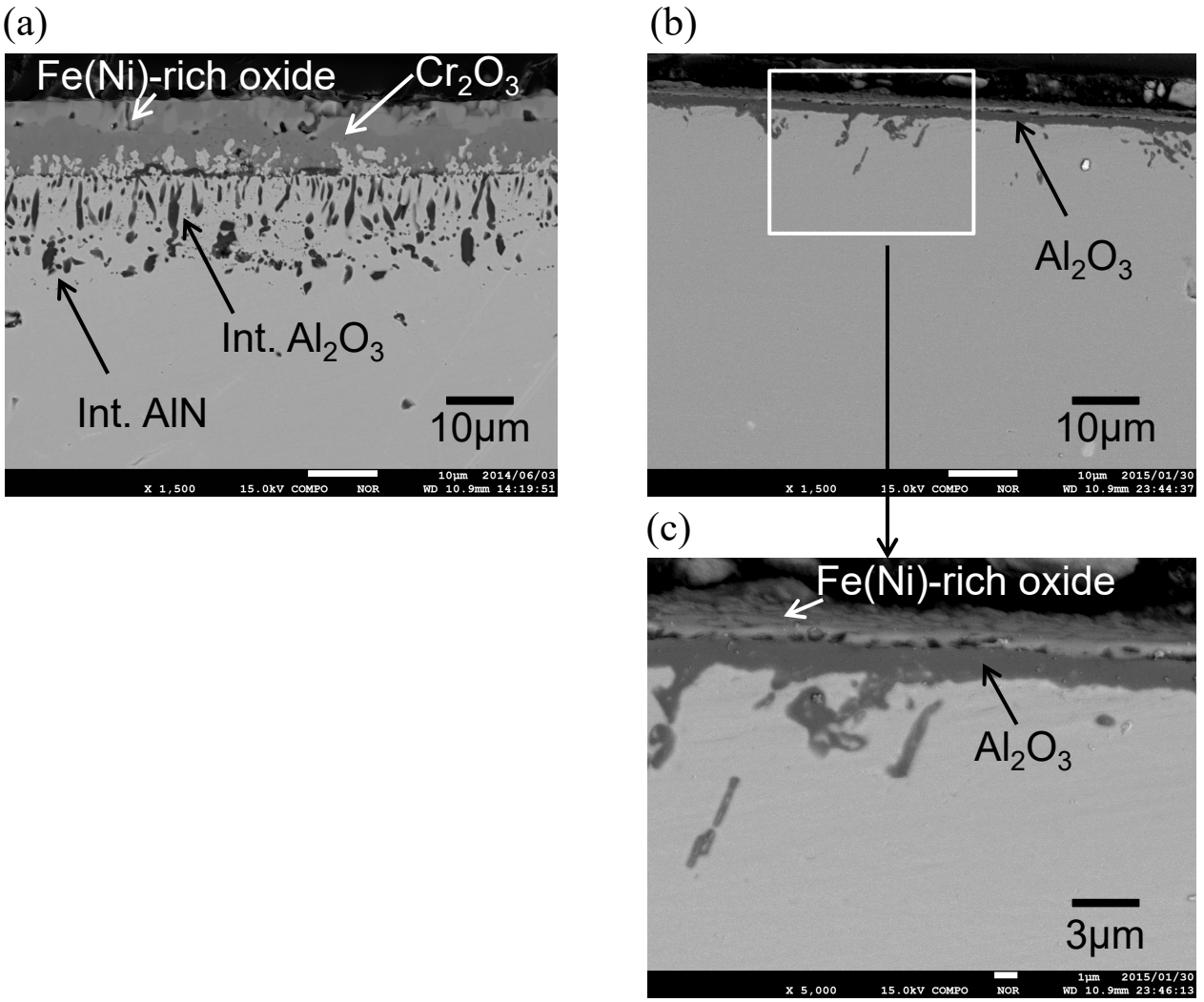

Fig. 5 Cross-sections of oxide scale formed on (a) Fe-17Ni-17Cr-6Al-5Cu and (b) Fe-17Ni-15Cr-7.7Al-5Cu after 100h of oxidation in air at 1000 °C, (c) is enlarged image of (b)

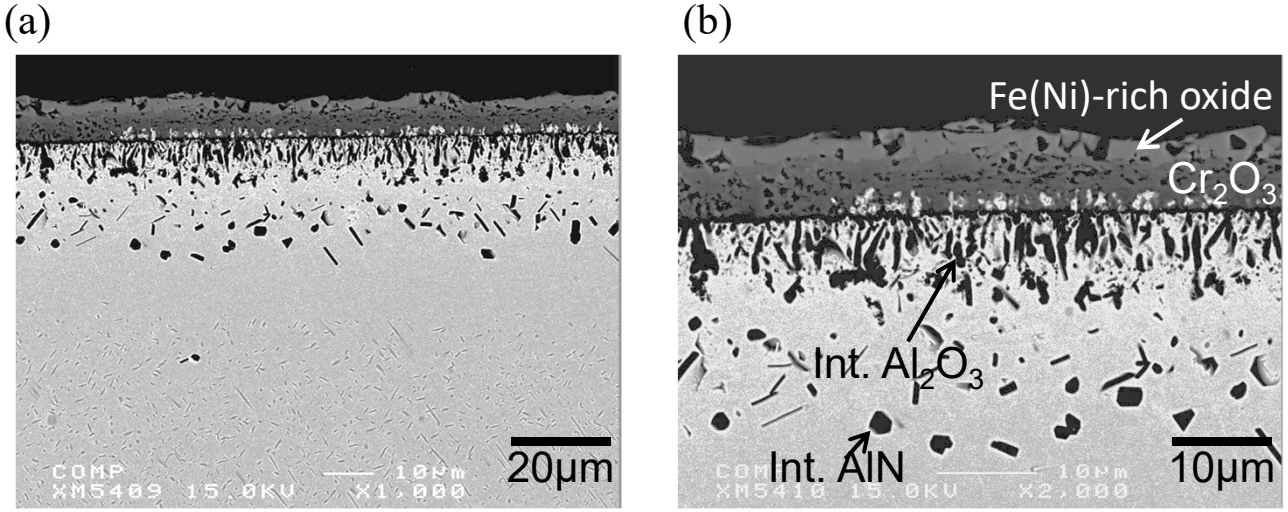

Fig. 6 Cross-sections of oxide scale formed on Fe-24Ni-17Cr-7.7Al. (b) is enlarged image of (a).

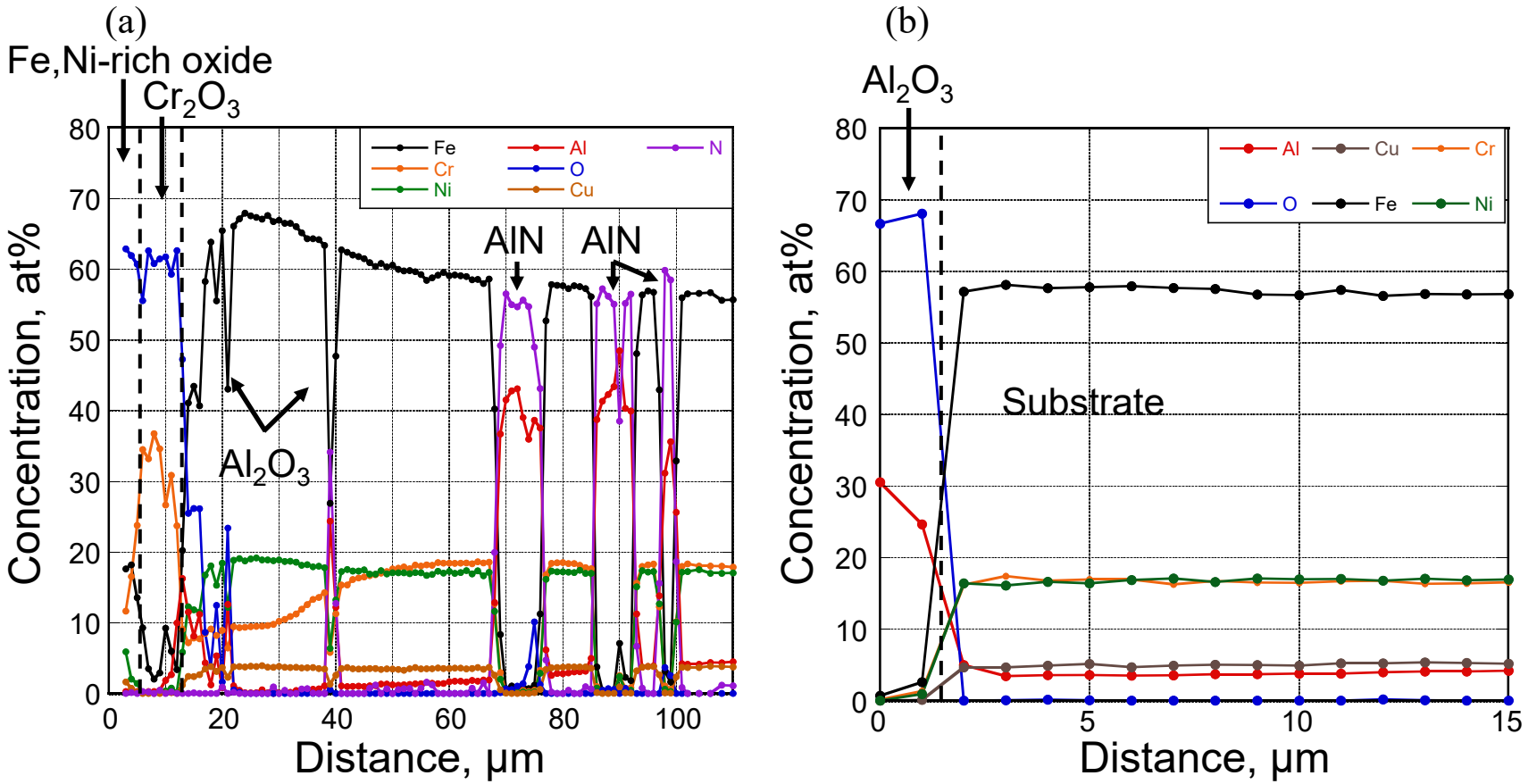

Fig. 7 EPMA concentration profiles of each element of (a) Fe-17Ni-17Cr-7.7Al-3.5Cu and (b) Fe-17Ni-17Cr-7.7Al-5Cu after 100h of oxidation in air at 1000 °C

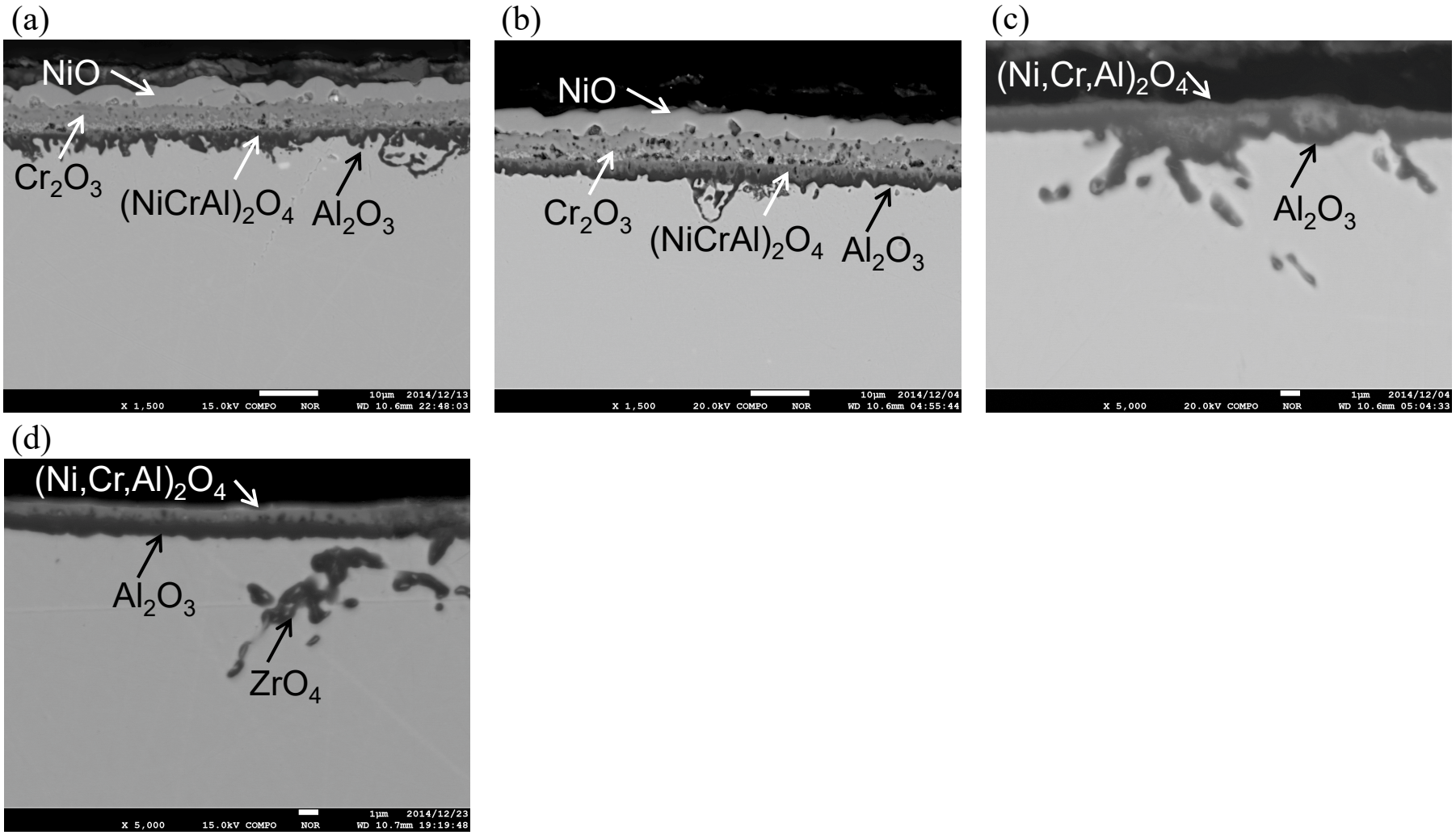

Fig. 8 Cross-sections of oxide scale formed on (a) Ni-17Cr-10Al, with (b) 5Cu, (c) 10Cu, and (d) 15Cu alloys after 100h of oxidation in air at 1000 °C

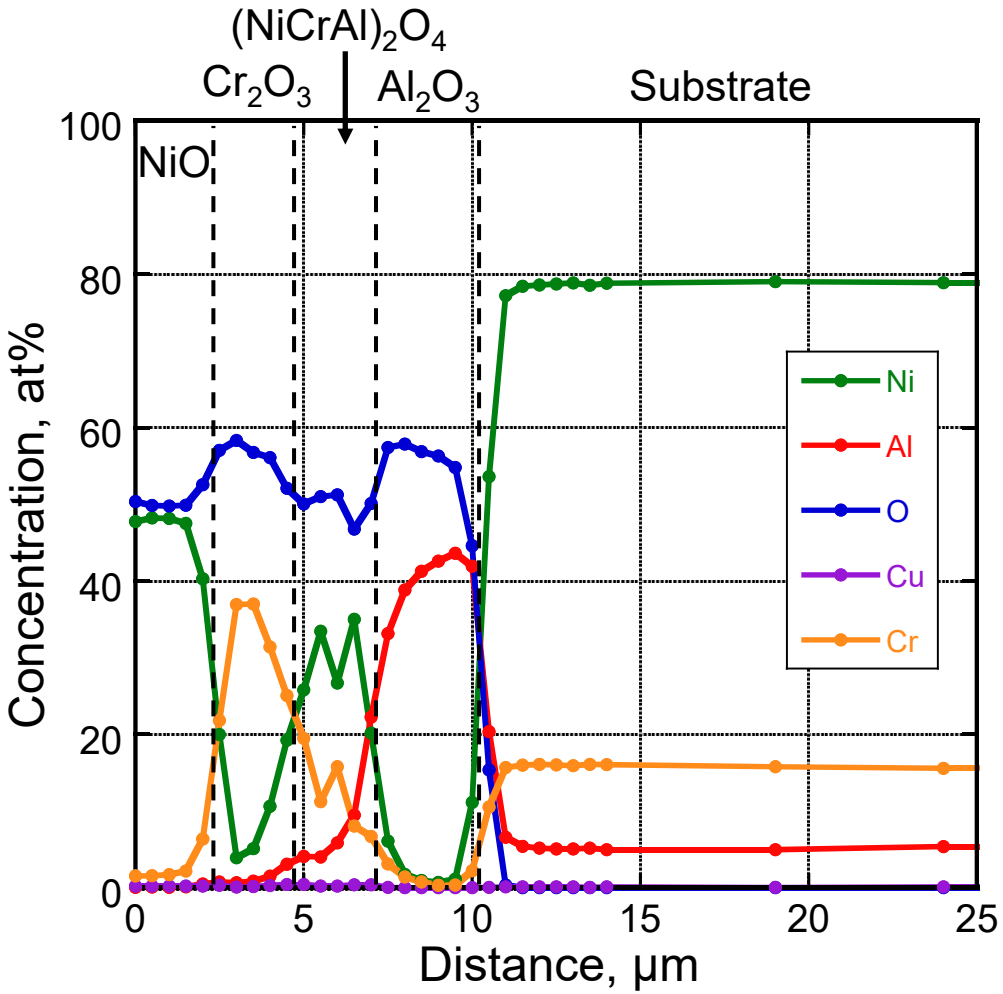

Fig. 9 EPMA concentration profiles of each element of 17Ni-17Cr-10Al after 100h of oxidation in air at 1000 °C

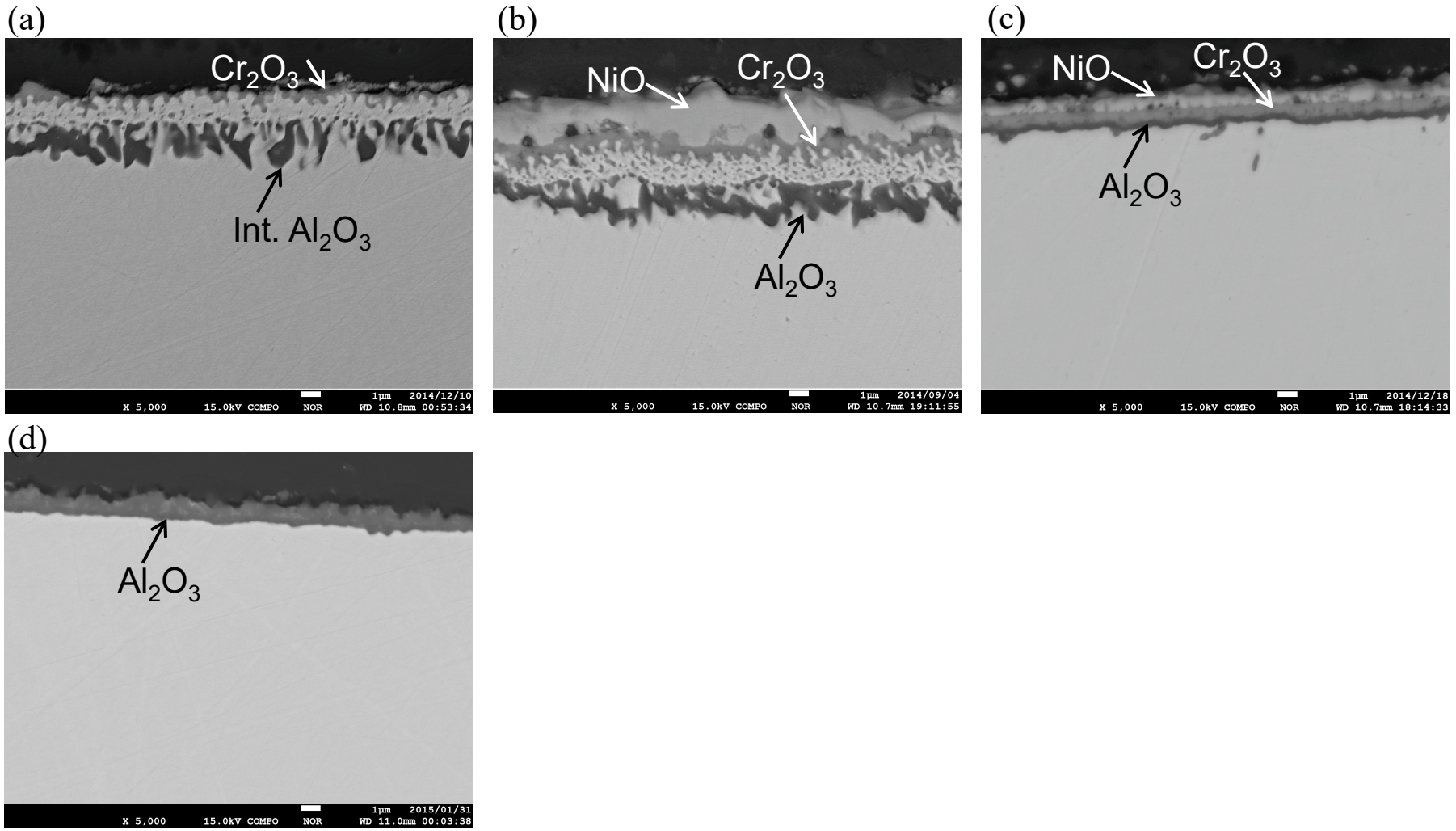

Fig. 10 Cross-sections of oxide scale formed on (a) Ni-17Cr-10Al, with (b) 5Cu, (c) 10Cu, and (d) 15Cu alloys after 4h of oxidation in air at 1000 °C

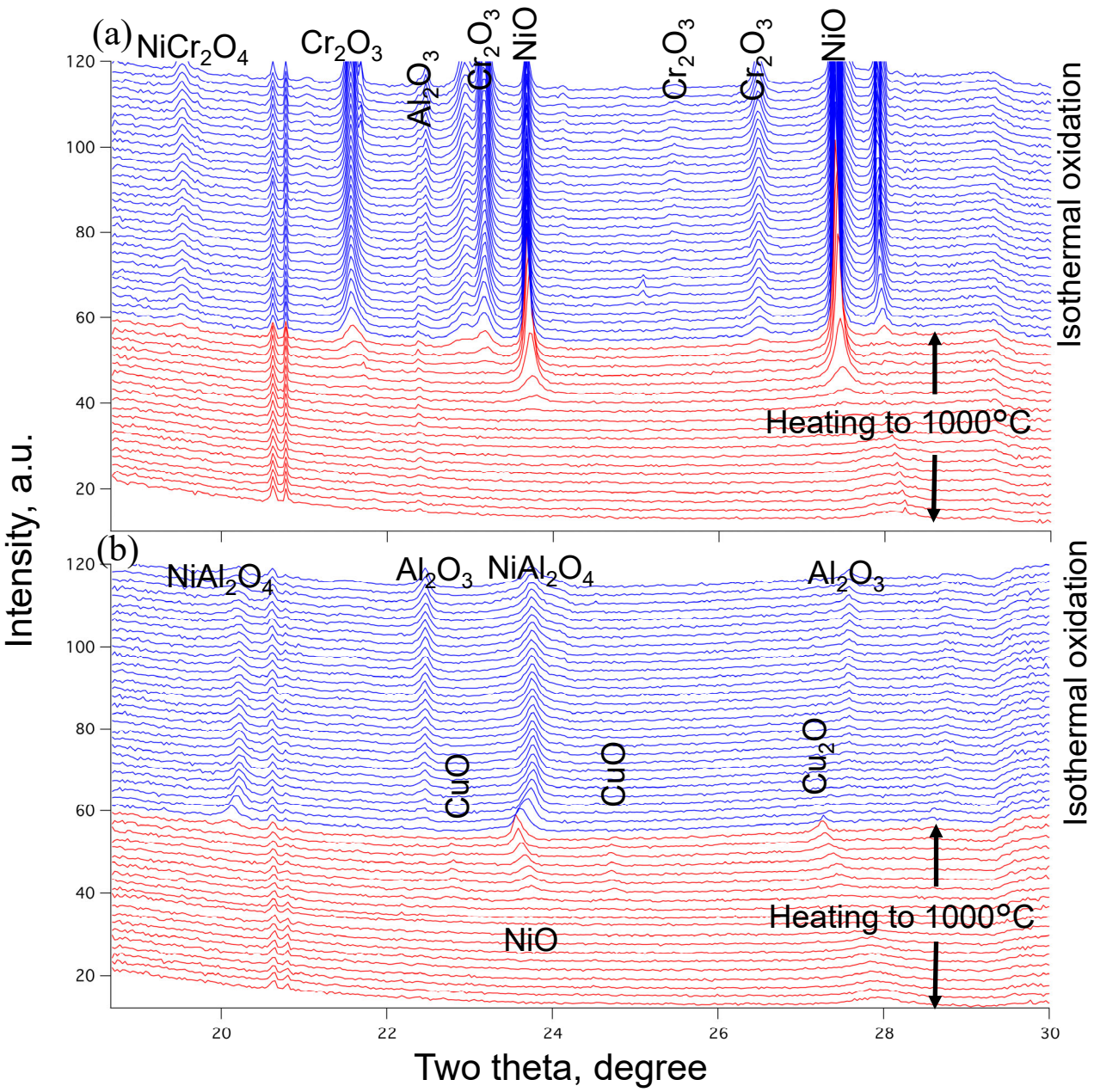

Fig. 11 In-situ HT-XRD patterns of (a)Ni-17Cr-10Al and (b)Ni-17Cr-10Al-15Cu alloys during heating followed by isothermal oxidation in air at 1000 °C

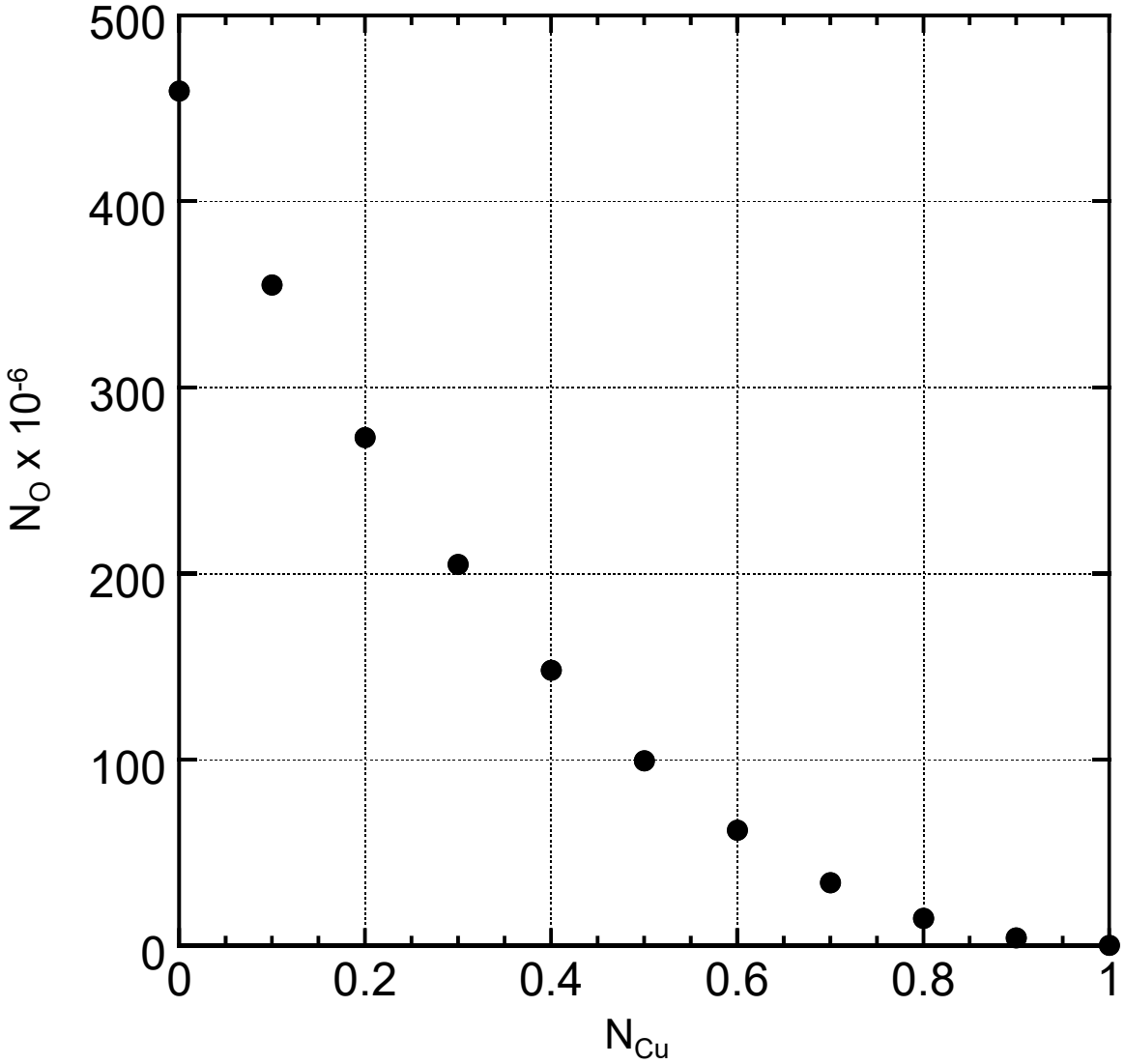

Fig. 12 Effect of Cu on the oxygen solubility in Ni-Cu system at 1000 °C

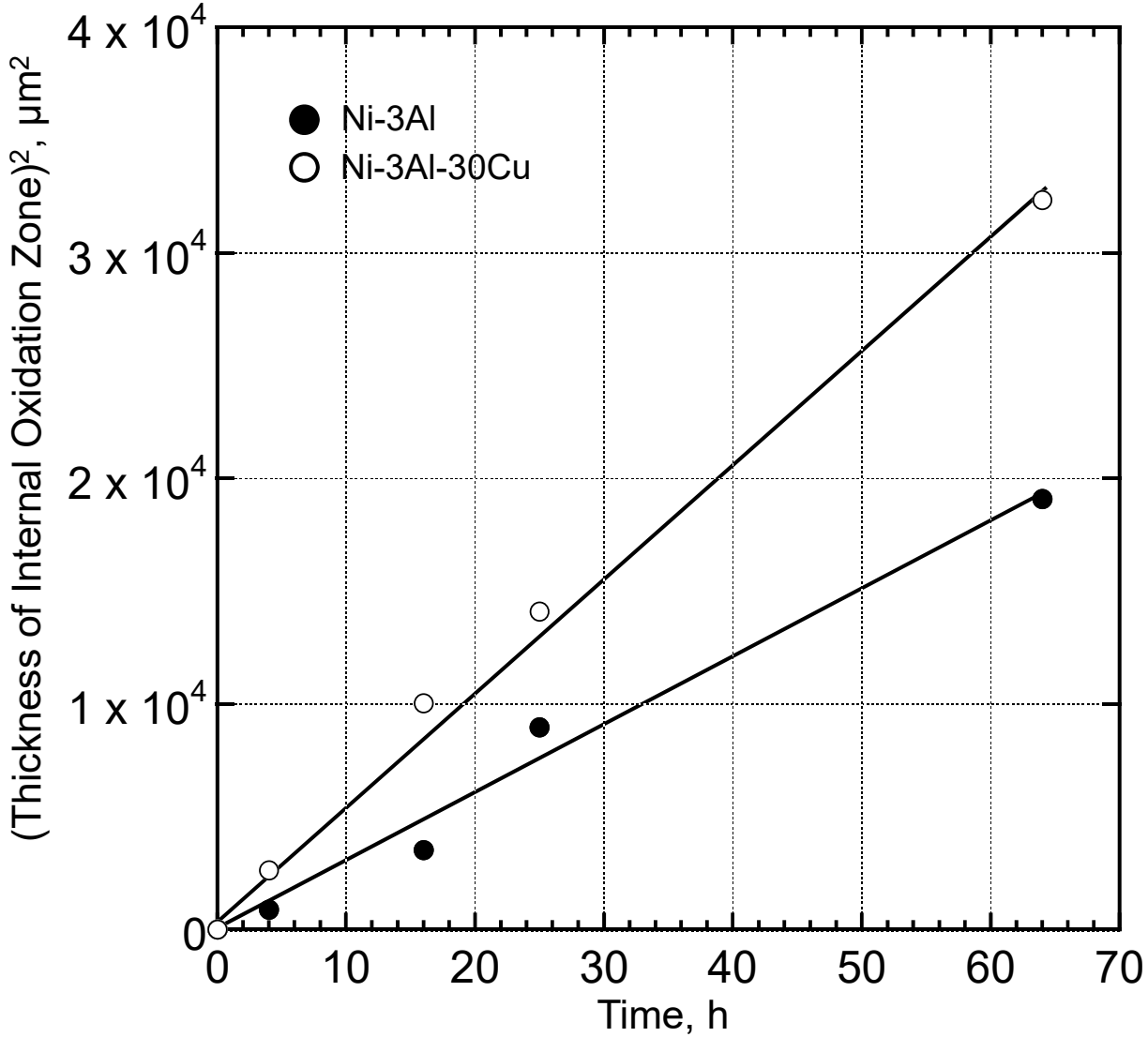

Fig. 13 Internal oxidation kinetics of Ni-3Al and Ni-3Al-30Cu at 1000 °C in Ni/NiO mixture

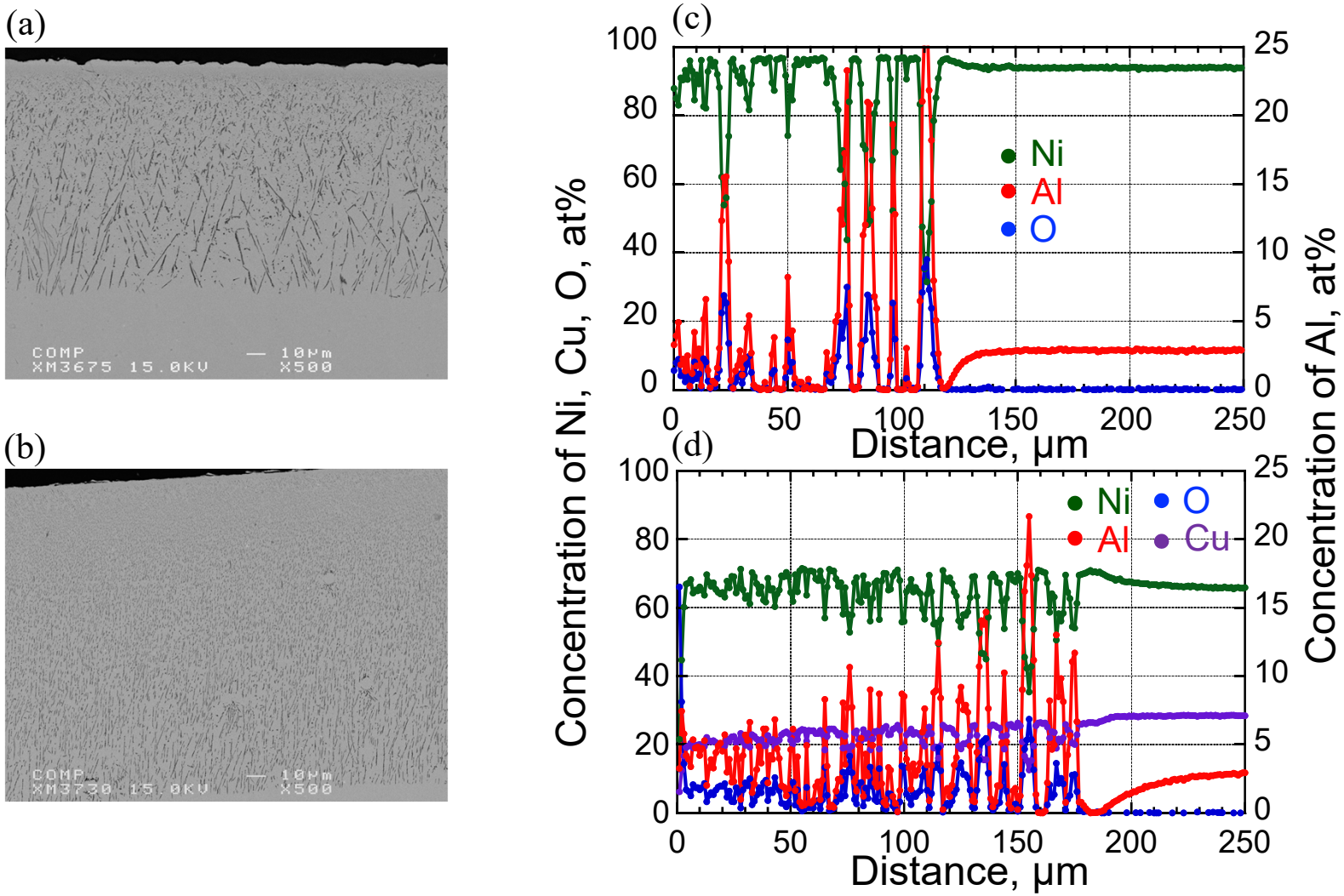

Fig. 14 Cross-sections of (a)Ni-3Al and (b)Ni-3Al-30Cu after internal oxidation for 64h at 1000 °C.
(c) and (d) are concentration profiles of each element of (a) and (b), respectively.

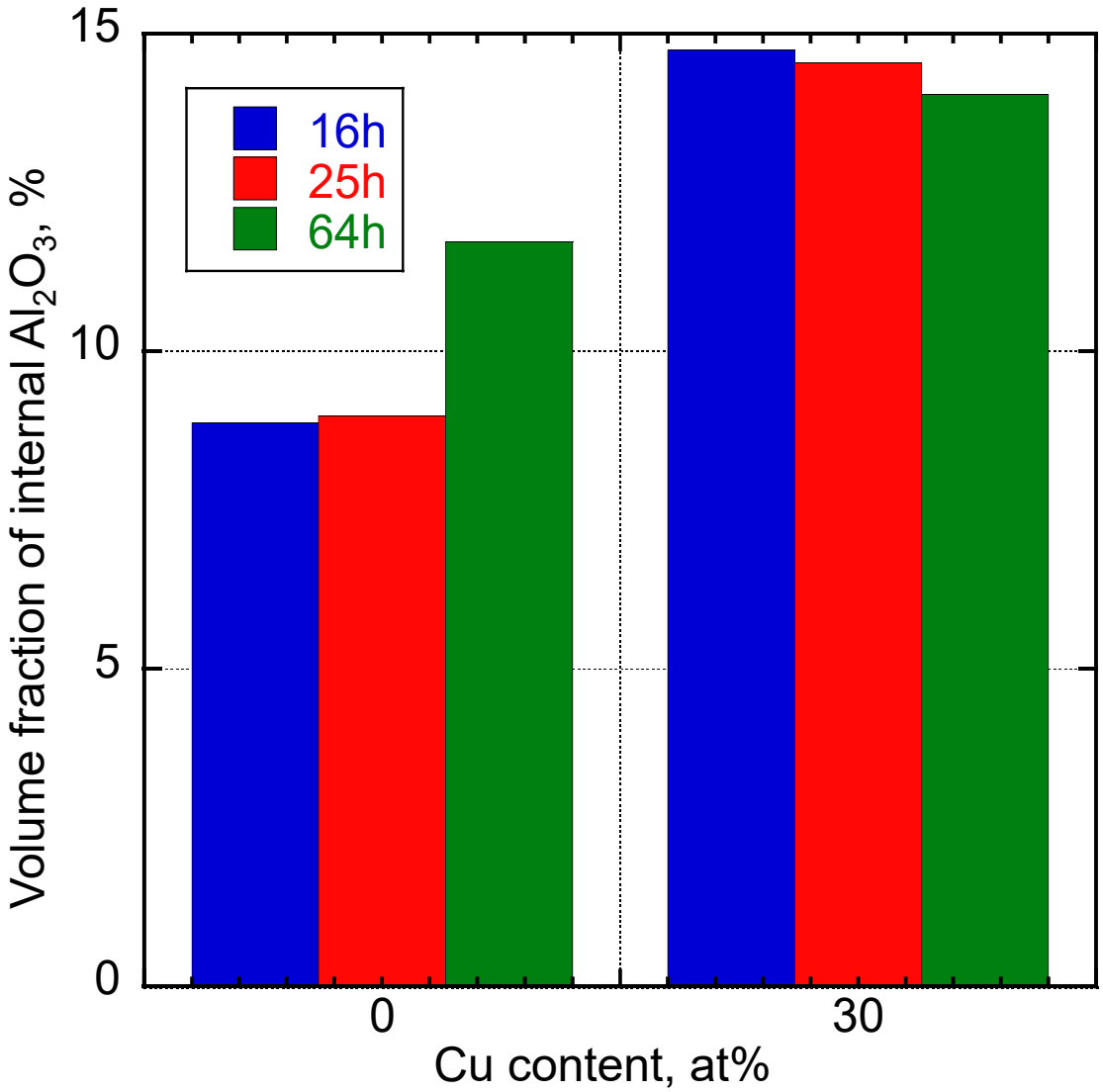

Fig. 15 Volume fraction of internal Al_2O_3 precipitates formed in Ni-3Al and Ni-3Al-30Cu alloys

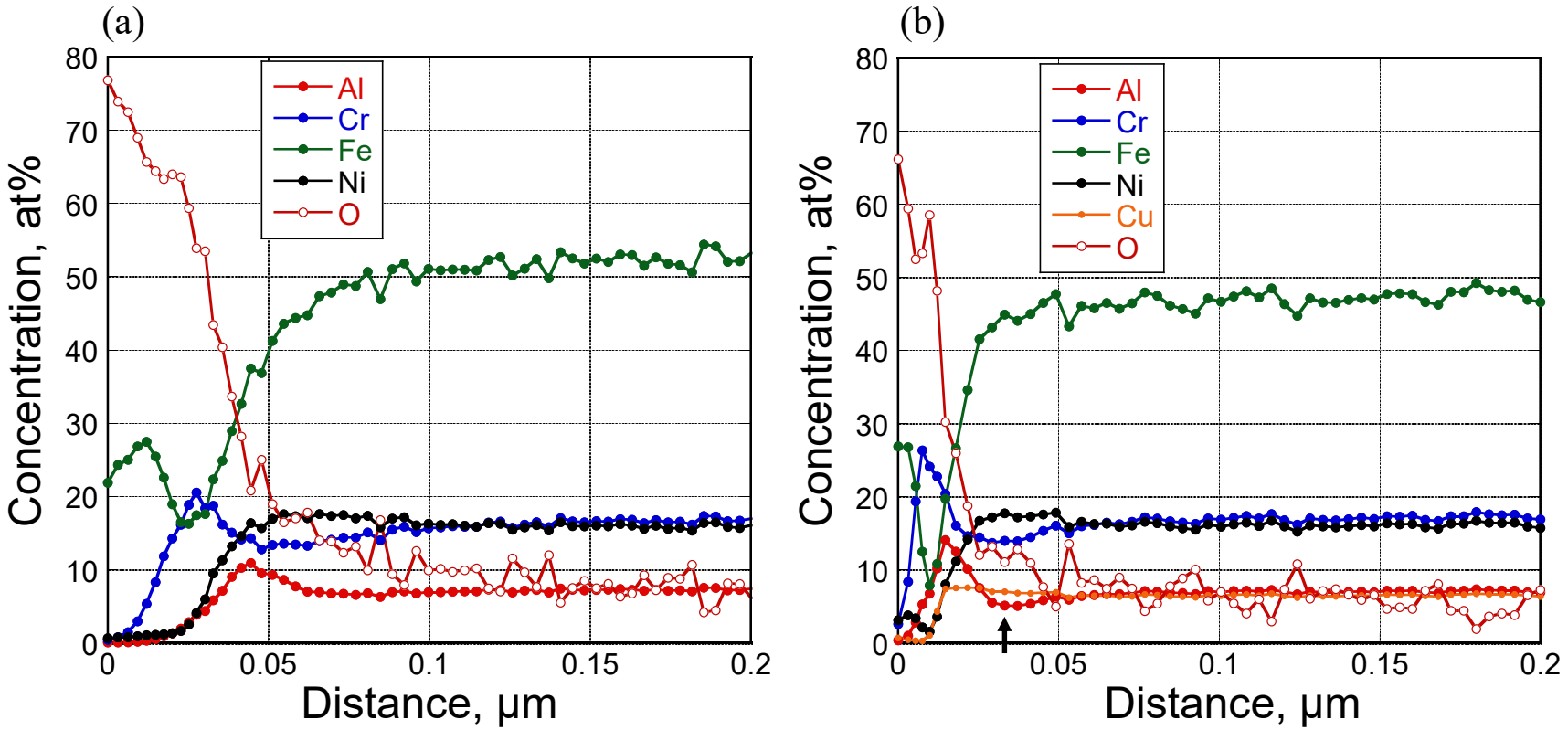

Fig. 16 GD-OES concentration profiles of each element of (a) Fe-17Ni-17Cr-7.7Al and (b) Fe-17Ni-15Cr-7.7Al-7Cu after 30s of oxidation in air at 1000 °C